Nanoscale

RSC Publishing

PAPER

View Article Online
View Journal | View Issue

Cite this: *Nanoscale*, 2013, **5**, 12518

Sol-hydrothermal synthesis and optical properties of Eu^{3+}, Tb^{3+}-codoped one-dimensional strontium germanate full color nano-phosphors

Liangwu Lin,[a] Xinyuan Sun,[b] Yao Jiang[a] and Yuehui He*[a]

Novel near-UV and blue excited Eu^{3+}, Tb^{3+}-codoped one dimensional strontium germanate full-color nano-phosphors have been successfully synthesized by a simple sol-hydrothermal method. The morphologies, internal structures, chemical constitution and optical properties of the resulting samples were characterized using FE-SEM, TEM, HRTEM, EDS, XRD, FTIR, XPS, PL and PLE spectroscopy and luminescence decay curves. The results suggested that the obtained Eu^{3+}, Tb^{3+}-codoped strontium germanate nanowires are single crystal nanowires with a diameter ranging from 10 to 80 nm, average diameter of around 30 nm and the length ranging from tens to hundreds micrometers. The results of PL and PLE spectra indicated that the Eu^{3+}, Tb^{3+}-codoped single crystal strontium germanate nanowires showed an intensive blue, blue-green, green, orange and red or green, orange and red light emission under excitation at 350–380 nm and 485 nm, respectively, which may attributed to the coexistent Eu^{3+}, Eu^{2+} and Tb^{3+} ions, and the defects located in the strontium germanate nanowires. A possible mechanism of energy transfer among the host, Eu^{3+} and Tb^{3+} ions was proposed. White-emission can be realized in a single-phase strontium germanate nanowire host by codoping with Tb^{3+} and Eu^{3+} ions. The Eu^{3+}, Tb^{3+}-codoped one-dimensional strontium germanate full-color nano-phosphors have superior stability under electron bombardment. Because of their strong PL intensity, good CIE chromaticity and stability, the novel 1D strontium germanate full-color nano-phosphors have potential applications in W-LEDs.

Received 8th August 2013
Accepted 29th September 2013

DOI: 10.1039/c3nr04185a

www.rsc.org/nanoscale

Introduction

Luminescent inorganic nanomaterials have attracted considerable interest for their tremendous potential applications as well as fundamental science research in many fields such as optics, optoelectronics, and biolabeling.[1–5] Recently, these inorganic nanophosphors have attracted much attention for use as a phosphor to convert the radiation of a near-UV or blue LED chip into white light.[6–9] Especially, nanophosphors with higher luminous efficiency, higher color rendering index and lower cost are the current challenges required in the field of W-LEDs.[10]

Phosphor is a key material and bottle-neck in solid-state illumination devices that use W-LEDs as the light source, which is often composed of a host and activator. The optical properties of the phosphors depend on the characteristics of the host and activator to some degree, such as the structure, photoelectric properties, and stability (including physical, chemical and thermal stability). Therefore, it is a key problem to choose a suitable host and activator for designing new high-efficiency and reliable phosphors for W-LEDs. For the host (in the size range greater than micrometers), generally, the top-priority characteristics are the structure and stability, while excellent photoelectric properties are often considered for the activator. It is well known that, compared to bulk materials, nanomaterials show excellent new physical properties, such as quantum size effects, small size effects, surface effects, coulomb blockade and quantum tunneling effects, and dielectric confinement effects,[11,12] often especially show excellent optical properties.[13–18] Therefore, recently, people have paid more and more attention to nanometer hosts. The aim is to obtain novel phosphors for W-LEDs by combining the excellent optical properties of the nanometer host and activator. So far, many nanometer hosts have been selected to study the optical properties for W-LEDs, such as silica nanowires,[19] ZnO nanowires,[20] $CaYAlO_4$ nanocrystals[21] Y_2O_3 nanocrystals.[22] It was found that the luminescent efficiency increases with decreasing size of the host[22–25] and more perfect emission spectra were obtained, which exhibit good CRI.[19,20]

In the past, most of the nano-host research focuses on nanoparticles, but there are very few studies on one-dimensional nano-hosts. Recently, one-dimensional nanomaterials have attracted more and more interest as their unique optical and electronic properties make them feasible of serving as the host of nano-phosphors.[19,20,26–28] In addition, the number of elements in the one-dimensional hosts is a key factor in controlling their functionalities and properties. In this regard,

[a]*State Key laboratory for Powder Metallurgy, Central south University, Changsha, Hunan 410083, People's Republic of China. E-mail: yuehui@mail.csu.edu.cn*

[b]*Department of Physics, Jinggangshan University, Ji'an Jiangxi 343009, People's Republic of China*

ternary one-dimensional nanomaterials used as a host for phosphors are more appealing than conventional binary one-dimensional nanomaterials, as ternary compositions offer broader options to tune the properties by adjusting the ratio of the three elements by doping.

Among the ternary one-dimensional nanomaterials, ternary germanate, such as $CuGeO_3$, Zn_2GeO_4, $In_2Ge_2O_7$, $Cd_2Ge_2O_6$, $Ca_2Ge_7O_{16}$, $BaGe_4O_9$ and $SrGe_4O_9$ have been reported for their applications in catalysis, magnetism, optical devices and sensors.[29–35] Several methods have been developed for the synthesis of germanate one-dimensional nanomaterials, including surfactant-assisted hydrothermal synthesis,[29,30,35,36] a solvothermal method[31] and the thermal evaporation method.[34] So far, there have been very few reports on the synthesis of rare earth ion doped germanate one-dimensional nanomaterials used as nano-phosphors, especially full-color nano-phosphors.

In this paper, we report novel near-UV and blue excited Eu^{3+}, Tb^{3+}-codoped one-dimensional strontium germanate full-color nano-phosphors which were synthesized by a facile sol-hydrothermal route. The Eu^{3+}, Tb^{3+}-codoped single crystal strontium germanate nanowires showed an intensive blue, blue-green, green, orange and red or green, orange and red light emission under excitation at 350–380 nm and 485 nm, respectively. The morphology, crystal structure, composition and luminescence properties of these phosphors were analyzed using powder X-ray diffraction (XRD), X-ray photoelectron spectroscopy (XPS), inductively coupled plasma mass-spectrometry (ICP-MS), photoluminescence (PL) spectroscopy, photoluminescence excitation (PLE) spectroscopy, FTIR, field emission-scanning electron microscopy (FE-SEM), transmission electron microscopy (TEM), high resolution TEM (HRTEM) and luminescence decay curves. A possible mechanism of energy transfer among the strontium germanate nanowires host, Eu^{3+} and Tb^{3+} ions is also proposed.

Results and discussion

After the hydrothermal process, the products were taken out of the autoclave and put into a 100 ml beaker for one day. We found the products separated into two parts, as shown in Fig. 1 (a). Taking the upper part out of the beaker and putting it into a 250 ml beaker, we can observe clearly that the products are floccus, as shown in Fig. 1(b). The woolly cloudlike aggregations were filtered and washed with distilled water until the pH of the water was equal to 7, then dried at 80 °C in air, and, finally, white products were obtained, as shown in Fig. 1(c). The lower sediment was also filtered, washed and dried by in same way for comparison with the products in the upper part. The composition, phase purity and morphology of the Eu^{3+}, Tb^{3+}-codoped strontium germanate nanowires and the lower sediment were investigated by XRD and FE-SEM. The morphology and size of the products in the upper part and the lower sediment are shown by the FE-SEM micrograph (from low magnification to higher magnification) in Fig. 2. FE-SEM (Fig. 2(a) and (b)) observations reveal that the product in the upper part consists of flexible wire-like structures. The obtained nanowires are about 10–80 nm in diameter (average diameter of 30 nm) and up to hundreds of micrometers in length, and possess smooth surfaces and uniform diameter along the entire length. No other particles can be seen, indicating the purity is very high. However, the lower sediment (Fig. 2(c) and (d)) consists of wire-like structures with larger diameters than those in the upper part, and some large particles which may come from the unreacted raw materials.

The XRD patterns of the undoped strontium germanate nanowires, the Eu^{3+}, Tb^{3+}-codoped strontium germanate nanowires, the lower sediment shown in Fig. 1(a), the Joint

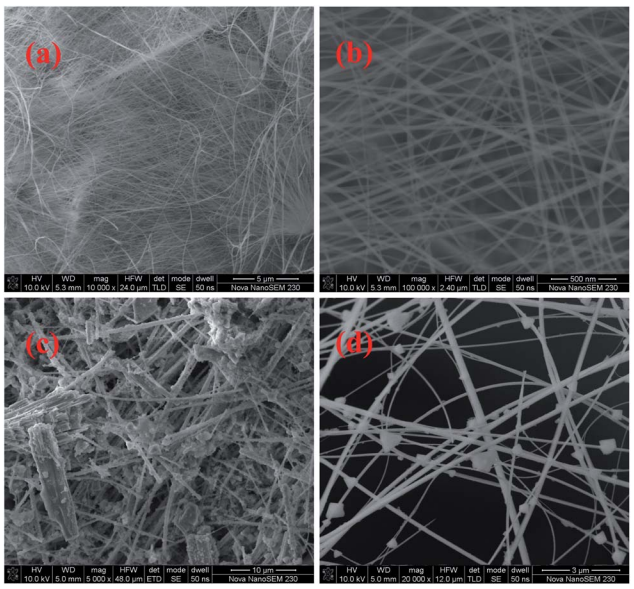

Fig. 2 FE-SEM images of Eu^{3+}, Tb^{3+}-codoped strontium germanate nanowires at different magnifications: (a)×10 000; (b)×100 000, and the lower sediment shown in Fig. 1(a): (c)×5000; (d)×20 000.

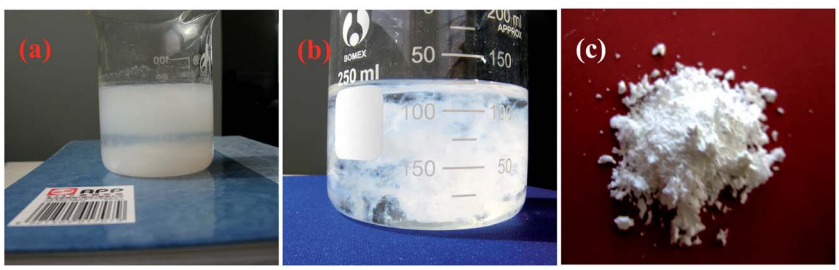

Fig. 1 The digital photograph of (a) the as-grown Eu^{3+}, Tb^{3+}-codoped strontium germanate nanowires after storage in a beaker for a day; (b) the product of the upper part in (a); and (c) the dried product at 80 °C in air after washing with deionized water.

Committee on Powder Diffraction Standards (JCPDS) card no. 86-1299 and JCPDS card no. 36-1463 of germanium oxide are shown in Fig. 3(a)–(e), respectively. For the undoped strontium germanate nanowires (Fig. 3(a)), the diffraction peaks can be well indexed to the hexagonal phase of $SrGe_4O_9$ ($a = b = 11.34$ Å, $c = 4.75$ Å, $V = 528.99$ Å^3) as reported in the literature (JCPDS card no. 86-1299, Fig. 3(d)). In the case of the Eu^{3+}, Tb^{3+}-codoped strontium germanate nanowires (Fig. 3(b)), the characteristic diffractions of the hexagonal phase of $SrGe_4O_9$ are still obvious, and no other phases can be detected. In the case of the lower sediment shown in Fig. 3(c), the characteristic diffractions of the hexagonal phase of $SrGe_4O_9$ are also still obvious. However, when compared to the undoped sample carefully, a hexagonal phase of GeO_2 can be observed in the lower sediment, which can be well indexed with the JCPDS card no. 36-1463 (space group *P*3221(154), Fig. 3(e)), indicating the particles shown in Fig. 2(c) and (d) are unreacted germanium oxide. The calculated lattice constants using the Jade 6.0 program, for example, $a = b = 11.31387$ Å, $c = 4.71249$ Å, $V = 522.4$ Å^3 for the Eu^{3+}, Tb^{3+}-codoped strontium germanate nanowires, $a = b = 11.3244$ Å, $c = 4.71303$ Å, $V = 523.34$ Å^3 for the lower sediment, show good compatibility with the standard data of $a = b = 11.34$ Å, $c = 4.75$ Å, $V = 528.99$ Å^3 for undoped strontium germanate nanowires (space group *P*321(150)). Moreover, it is found that incorporation of the Eu^{3+} and Tb^{3+} ions into strontium germanate results in a slight shrinkage of the lattice constants and the unit cell volume due to the smaller radius of Eu^{3+} (95 pm) and Tb^{3+} (92.5 pm) than that of Sr^{2+} (113 pm), indicating the Eu^{3+} and Tb^{3+} ions have been incorporated into the host lattice of $SrGe_4O_9$ and do not change the crystal structure. The results of ICP-MS analysis show that the actual doping concentration of Tb^{3+} and Eu^{3+} in the Eu^{3+}, Tb^{3+}-codoped strontium germanate nanowires is 2.08 and 7.86 wt%, respectively, which is much closer to the molar ratio of Tb^{3+}/Eu^{3+} (around 1/4) in the raw materials.

In order to study the morphology, composition and microstructure of the Eu^{3+}, Tb^{3+}-codoped strontium germanate nanowires in detail, the TEM, HRTEM and EDS were performed on a field emission high-resolution transmission electron microscope. The results are shown in Fig. 4. Fig. 4(a) shows typical low magnification TEM images of the Eu^{3+}, Tb^{3+}-codoped strontium germanate nanowires which are similar to those of the SEM observations, revealing that the periphery of the nanowires are very smooth and clean with the diameter ranging from 20 to 35 nm. The inset shown in Fig. 4(a) indicated that there is not any coating of nanoparticles on the growth tip, which is often seen on the tip of one-dimensional nanomaterials obtained by catalyst-assisted growth. The compositions of the nanowires were measured by EDS which was equipped on the JEM-2100F field emission high-resolution transmission electron microscope, as shown in Fig. 4(b). The EDS data reveal the presence of C, O, Sr, Ge, Eu and Tb, indicating that the Eu and Tb have entered the $SrGe_4O_9$ crystal lattice.

Fig. 4(c) is a typical HRTEM image of the Eu^{3+}, Tb^{3+}-codoped strontium germanate nanowires, and the inset corresponds to a fast Fourier transformation (FFT) image of the zone covered by dashed square. After removing unwanted noise and enhancing periodic elements of the image through the technology of Fourier masking provided by Gatan, Inc., an inverse fast Fourier transformation was performed, and the corresponding image is shown in Fig. 4(d). From Fig. 4(d), the atomic arrangement can be seen clearly, with a *d* spacing of 0.468 nm, corresponding to the (001) plane of the hexagonal $SrGe_4O_9$ phase, indicating that the nanowires grow along the [001] direction and possesses a perfect crystal structure with few structural defects such as dislocations and stacking faults, although some Eu and Tb atoms have entered the crystal lattice. The results demonstrate that the method employed in this work is efficient in doping rare earth ions into the crystal lattice of strontium germanate

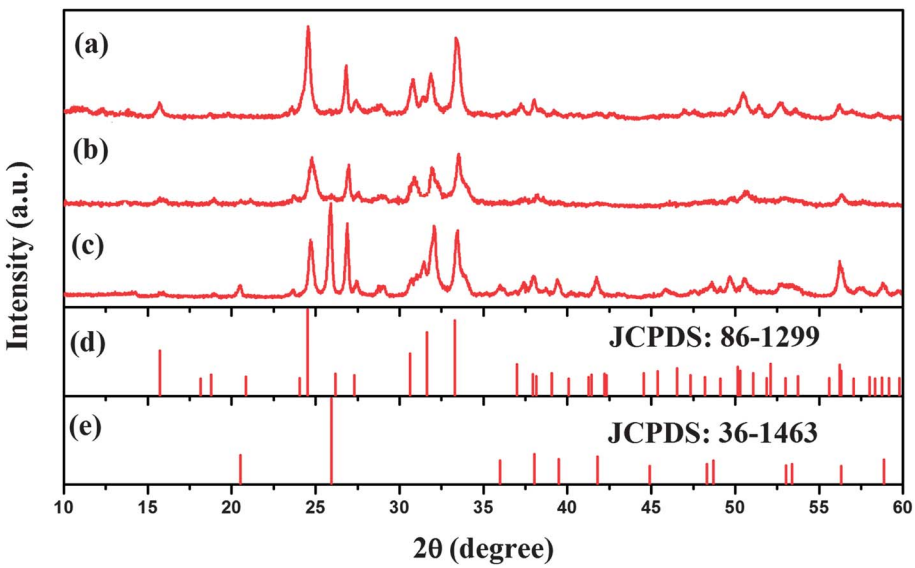

Fig. 3 XRD pattern of (a) undoped and (b) Eu^{3+}, Tb^{3+}-codoped strontium germanate nanowires; (c) the sediment in the bottom part in Fig. 1(a); (d) the Joint Committee on Powder Diffraction Standards (JCPDS) card no. 86-1299 and (e) JCPDS card no. 36-1463.

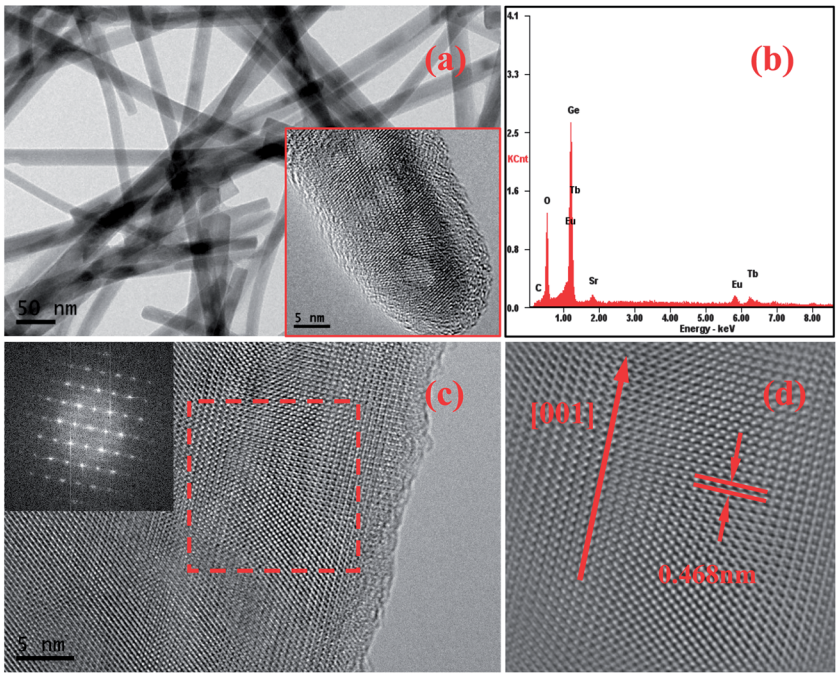

Fig. 4 TEM image, the inset is the HRTEM of the growth tip (a), EDS spectrum (b), HRTEM image (c) of Eu^{3+}, Tb^{3+}-codoped strontium germanate nanowires. The inset is the corresponding FFT pattern of the specific region marked by the dashed square in (c), and (d) the corresponding filtered inverse FFT image of the inset in (c).

nanowires uniformly. Meanwhile, it is noteworthy that there is no significant deformation in the Eu^{3+}, Tb^{3+}-codoped one-dimensional strontium germanate nano-phosphors under electron bombardment, suggesting the nano-phosphors have superior stability.

Curve (a) and (b) in Fig. 5 show the infrared percentage transmission spectra of (a) undoped and (b) Eu^{3+}, Tb^{3+}-codoped strontium germanate nanowires in the 400–2000 cm^{-1} range, respectively. In curve (a), the peaks at 860 and 573 cm^{-1} are attributed to the Ge–O–Ge antisymmetrric stretching vibration mode and bending vibration modes, respectively. Compared with the bulk GeO_2 (880 and 529 cm^{-1}),[37] the two vibration modes have a redshift and blueshift of 20 and 44 cm^{-1}, respectively. It is because the influence of Sr^{2+} on the Ge–O–Ge bond increased when the reaction was carried out continuously in a sealed Teflon-lined autoclave employing $C_4H_6O_4Sr\cdot 1/2H_2O$ and GeO_2 as the reactants, and the intensity of the Ge–O–Ge bond was weakened little by little. The weakening effect of Sr^{2+} on the Ge–O–Ge bond caused it to break, and finally, form the Ge–O–Sr bond causing a change in the coordination number of Ge from 4 to 6.[38–41] The two minus charges of the GeO_6 octahedra are balanced by the localization of Sr^{2+} ions.[42] Therefore, the antisymmetrric stretching vibration mode of the Ge–O–Ge bond shifts gradually toward lower wavenumbers as the weakening increases.[43,44] The higher the Ge–O–Sr bond content the greater the shift and the GeO_6/GeO_4 molar ratio which is in

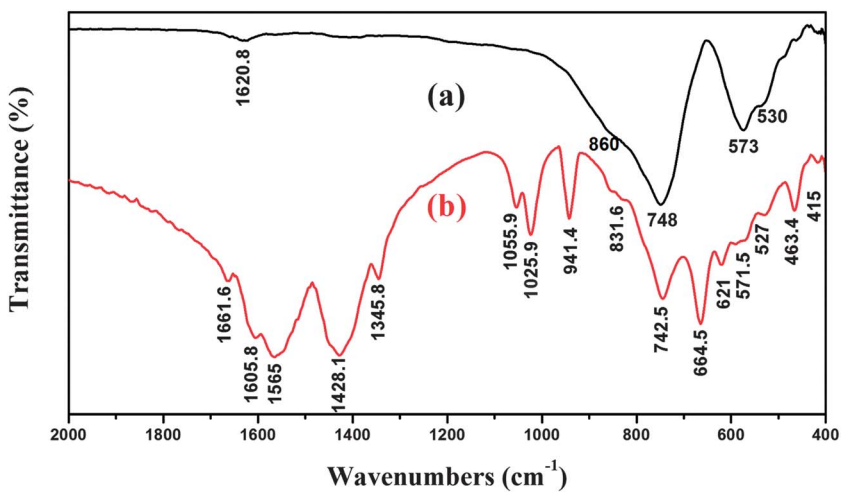

Fig. 5 FTIR spectra of (a) strontium germanate nanowires and (b) Eu^{3+}, Tb^{3+}-codoped strontium germanate nanowires.

good accord with the general notion that an increase in coordination from XO_4 to XO_6 causes a decrease in X–O–X stretching frequency.[45] Meanwhile, the bending vibration mode of the Ge–O–Ge shifts gradually toward higher wave numbers because the action along the stretching direction of the Ge–O–Ge bond increases and must absorb higher energy to make it bend.[37] Those are the reasons why the stretching vibration and bending vibration modes of the Ge–O–Ge bond shift toward lower numbers and higher numbers, respectively. The peaks at 748 and 530 cm^{-1} are attributed to stretching vibration and bending vibration modes of the Ge–O–Sr bond which indicates that the nanowires are strontium germanate nanowires. The peak located at 1620.8 cm^{-1} originated from the bending vibration modes of the absorbent H_2O. Compared with curve (a), the curve (b) shows some differences: (1) the intensity of the absorption peaks shown in curve (b) in the 400–2000 cm^{-1} range is higher than that of curve (a); (2) some new absorption peaks attributed to Eu–O or Tb–O bonding are observed, such as 664.5, 621, 463.4 and 415 cm^{-1}, indicating that the Eu and Tb have entered the strontium germanate nanowires; (3) peaks located at 1605.8, 1565, 1428.1 and 1345.8 cm^{-1}, respectively, are assigned to the carboxylate (O–C=O) originating from the CH_3COO– residue in the product,[30] while the new absorption peaks at 1055.9, 1025.9 and 941.4 cm^{-1} are attributed to the ammonia containing compound or C–O–C; (4) the anti-symmetrric stretching and bending vibration of the Ge–O–Ge bonds located at 860 and 573 cm^{-1} redshift to 831.6 and 571.5 cm^{-1}, respectively, while the stretching and bending vibrations of the Ge–O–Sr bond located at 748 and 530 cm^{-1} also redshift to 742.5 and 527 cm^{-1}, respectively. These redshift

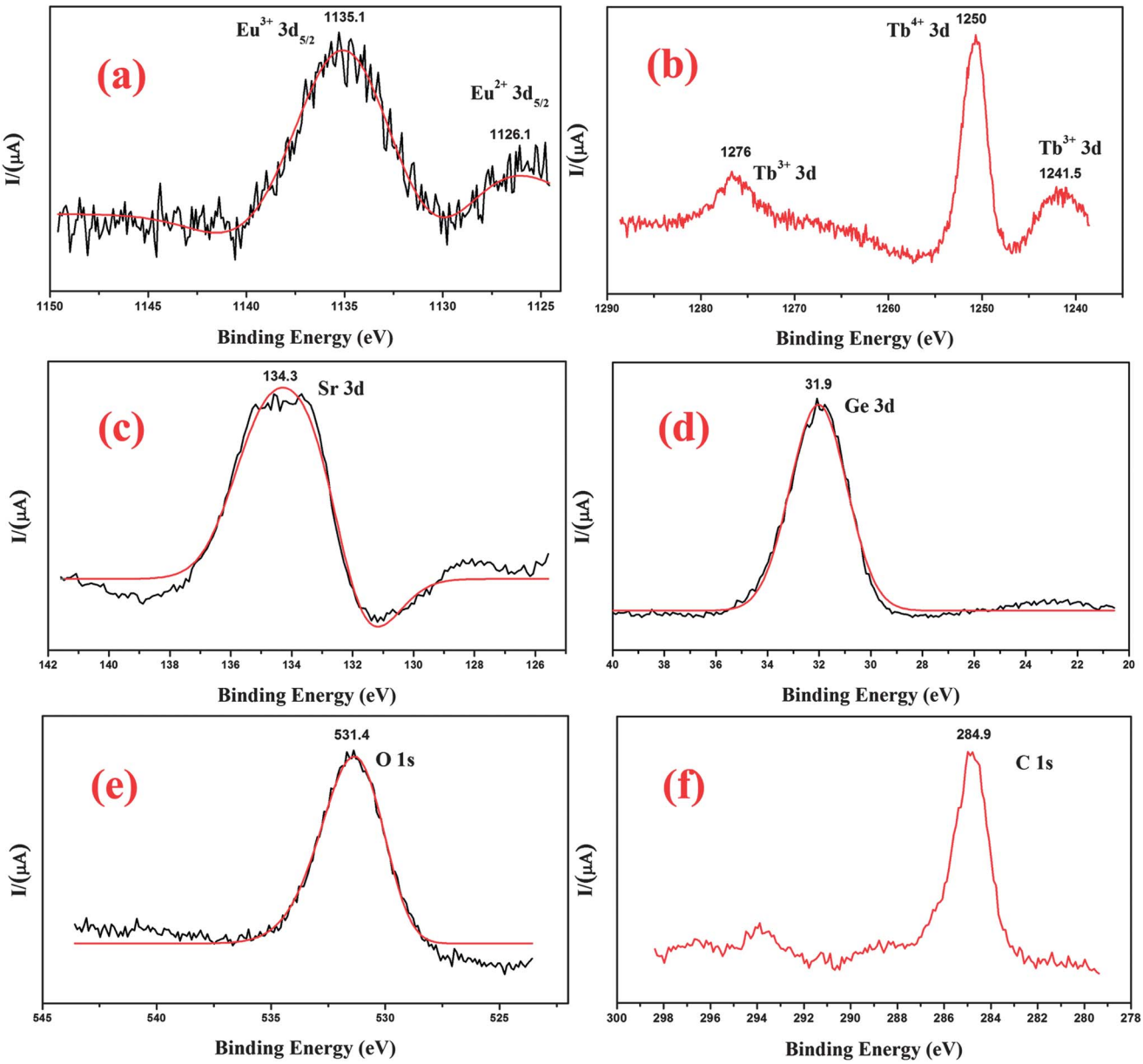

Fig. 6 XPS spectrum of the Eu^{3+}, Tb^{3+}-codoped strontium germanate nanowires: (a) Eu (3d); (b) Tb (3d); (c) Sr (3d); (d) Ge (3d); (e) O (1s); (f) C (1s).

phenomena may be related to the progressive replacing of Sr^{2+} by Eu^{3+} and Tb^{3+} ions. As is known, the ionic radii of Eu^{3+} (95 pm) and Tb^{3+} (92.5 pm) are smaller than that of Sr^{2+} (113 pm) while the ionic potential (φ) of Eu^{3+} (3.15) and Tb^{3+} (3.25) are higher than that of Sr^{2+} (1.77). Generally, the ionic potential can be estimated using the following equation $\varphi = Z/r$, where Z is the electric charge number of ion, and r is the ion radius (pm). Therefore, Eu^{3+} and Tb^{3+} have higher attractive force towards the groups which are closed about them, such as O^{2-}, $[GeO_4]$ and $[GeO_6]$, than Sr^{2+}. So, when some of the Sr^{2+} is replaced by Eu^{3+} and Tb^{3+} ions, the stretching vibration modes of the Ge–O–Ge and Ge–O–Sr bonds in the codoped strontium germanate nanowires shift toward lower wave numbers as a result of the higher weakening amplitude of the Ge–O–Ge bond. However, the bending vibration mode of the Ge–O–Ge and Ge–O–Sr also shift toward lower wave numbers, 1.5 and 3 cm^{-1}, respectively, instead of higher wave numbers, which is in contradiction with the undoped strontium germanate nanowires.

X-ray photoelectron spectroscopy (XPS) has been used as a powerful tool to determine the surface chemical composition of the Eu^{2+}, Tb^{3+}-codoped strontium germanate nanowires and the valence states of the various species present in it. The results are shown in Fig. 6(a)–(f). According to the XPS results, there are Sr, Ge, O, C, Eu and Tb elements on the surface of the Eu^{2+}, Tb^{3+}-codoped strontium germanate nanowires. The XPS spectrum of the Eu $3d_{5/2}$ core level of the Eu^{2+}, Tb^{3+}-codoped strontium germanate nanowires is shown in Fig. 6(a) along with the spectra of the typical Eu^{2+} (1126.1 eV) and Eu^{3+} (1135.1 eV), indicating that the Eu^{2+} and Eu^{3+} ions exist together non-equivalently in host material. Since the areas of Eu^{2+} and Eu^{3+} in the XPS spectra are proportional to the concentration of Eu, we can deduce that the ratio of Eu^{3+} ions is higher than that of Eu^{2+} ions in the host. The Tb^{3+} 3d (1241.5 and 1276 eV) and Tb^{4+} 3d (1250 eV) core level were also found in the Eu^{3+}, Tb^{3+}-codoped strontium germanate nanowires, indicating that Tb^{3+} and Tb^{4+} ions coexist in it, as shown in Fig. 6(b). The Sr 3d, Ge 3d, O 1s and C 1s core level peaks are located at 134.3, 31.9, 531.4 and 284.9 eV, as shown in Fig. 6(c)–(f), respectively. The C 1s originated from the absorbed organic groups on the surface of the Eu^{2+}, Tb^{3+}-codoped strontium germanate nanowires, which is in good accord with the FT-IR results.

The successfully synthesized Eu^{3+}, Tb^{3+}-codoped $SrGe_4O_9$ nanowires exhibit good luminescence properties and a high luminous efficiency. Fig. 7(a) and (b) show the excitation spectra monitoring the emission of Eu^{3+} at 612 nm and Tb^{3+} at 543 nm, respectively. As seen from Fig. 7(a), the excitation spectrum shows two main excitation bands. The broad band ranging from 200 to 320 nm with its center at ~250 nm is mainly associated with the charge-transfer state (CTS) moving from the 2p orbital of O^{2-} to the 4f orbital of Eu^{3+} ions. The position of the CTS band in the excitation spectrum is mainly determined by the covalency of the Eu–O bond and the coordination environment of Eu^{3+} as well.[46–48] The capped peak located in the range from 290–320 nm is an overtone of the light source. The other band extending from 330 to 550 nm is composed of a series of sharp lines. The peaks at 360, 378, 395, 414, 463, 531 nm, respectively, originated from the characteristic f → f transition of Eu^{3+} ions, corresponding to the transitions from the $^7F_0$ ground state to the different excited states of Eu^{3+}, such as 360 nm ($^7F_0 \rightarrow {}^5D_4$), 378 nm ($^7F_0 \rightarrow {}^5L_7$), 395 nm ($^7F_0 \rightarrow {}^5L_6$), 414 nm ($^7F_0 \rightarrow {}^5D_3$), 463 nm ($^7F_0 \rightarrow {}^5D_2$) and 531 nm ($^7F_1 \rightarrow {}^5D_1$). In addition, we also see some peaks at 340, 350 and 485 nm, respectively, which do not originate from the characteristic intra-4f transition of Eu^{3+} ions. Those may originate from the characteristic f → f transition of Tb^{3+} ions. In order to illuminate that, we also show the excitation spectra monitored with the emission of Tb^{3+} at 543 nm in Fig. 7(b). From Fig. 7(b), the excitation spectrum also shows two main excitation bands. One broad band ranging from 200 to 310 nm is originated from the characteristic f → d transition of Tb^{3+} ions, the other band is composed of seven peaks at 301, 318, 340, 350, 368, 376 and 485 nm, which are attributed to the intra-4f transition of Tb^{3+} ions, corresponding to 301 nm ($^7F_6 \rightarrow {}^3H_6$), 318 nm ($^7F_6 \rightarrow {}^5D_0$), 340 nm ($^7F_6 \rightarrow {}^5L_7$), 350 nm ($^7F_6 \rightarrow {}^5L_9$), 368 nm ($^7F_6 \rightarrow {}^5G_5$), 376 nm ($^7F_6 \rightarrow {}^5G_6$) and 485 ($^7F_6 \rightarrow {}^5D_4$), respectively. The capped peak located in the range 260–280 nm also is an overtone of the light source. Compared with Fig. 7(a) and (b), it was found that the excitation bands overlapped to some extent in the range of 320–420 nm and 450–500 nm, such as the peaks at 340, 350, 368, 376 and 485 nm, which suggest that the obtained one-dimensional nano-phosphor can be excited effectively by near-ultraviolet light-emitting diodes (UVLED) and blue light-emitting diodes (BLED). In addition, the excitation energy of Eu^{3+} is stronger than that of Tb^{3+} which is due to the fact that luminescence intensities of various rare-earth ions can be enhanced or quenched by the energy transfer from other codoped rare-earth ions.[32,45,49–51] Those illustrate the occurrence of energy transfer from Tb^{3+} to Eu^{3+} when they are codoped in the strontium germanate nanowires host and provide a necessary condition for synthesizing the single phase full-color phosphors.

Fig. 8(a)–(e) are the emission spectra of the Eu^{3+}, Tb^{3+}-codoped strontium germanate nanowires under excitation at 350, 376, 395, 465 and 485 nm, respectively, and the emission spectrum of undoped strontium germanate nanowires is shown in Fig. 8(f). Comparing Fig. 8(a) with Fig. 8(b), we can observed that both the emission spectra are composed of red (612, 649, 695 nm), orange (588 nm), green (543 nm), blue-green (488 nm), and blue (400–470 nm) light-emitting peaks. The red emission peaks are attributed to the typical $^5D_0 \rightarrow {}^7F_J$ ($J = 2$–4) transition emission of Eu^{3+}, including the strongest $^5D_0 \rightarrow {}^7F_2$ electric dipole transition at 612 nm, and the weak $^5D_0 \rightarrow {}^7F_3$ and $^5D_0 \rightarrow {}^7F_4$ transition emission at 649 and 695 nm, respectively. The orange emission peak at 588 nm might belong to the results of coactions of the $^5D_0 \rightarrow {}^7F_1$ magnetic dipole transition of Eu^{3+} and the $^5D_4 \rightarrow {}^7F_4$ transition emission of Tb^{3+}. The green and blue-green emission peaks at 543 and 488 nm originate from the $^5D_4 \rightarrow {}^7F_5$ and $^5D_4 \rightarrow {}^7F_6$ transition of Tb^{3+}. The broad blue-violet emission band maybe corresponds to the combined effects of the blue-violet emission of strontium germanate, the $^5D_3 \rightarrow {}^7F_J$ ($J = 4$–5) transition emission of Tb^{3+} and the d → f transition emission of Eu^{2+}.[49,50] This suggests that there may be three ions (Eu^{3+}, Eu^{2+} and Tb^{3+}) in the strontium germanate host, which is in good accord with the results of XPS mentioned above. Wu *et al.* thought that both Eu^{3+} and Tb^{3+} are conjugate

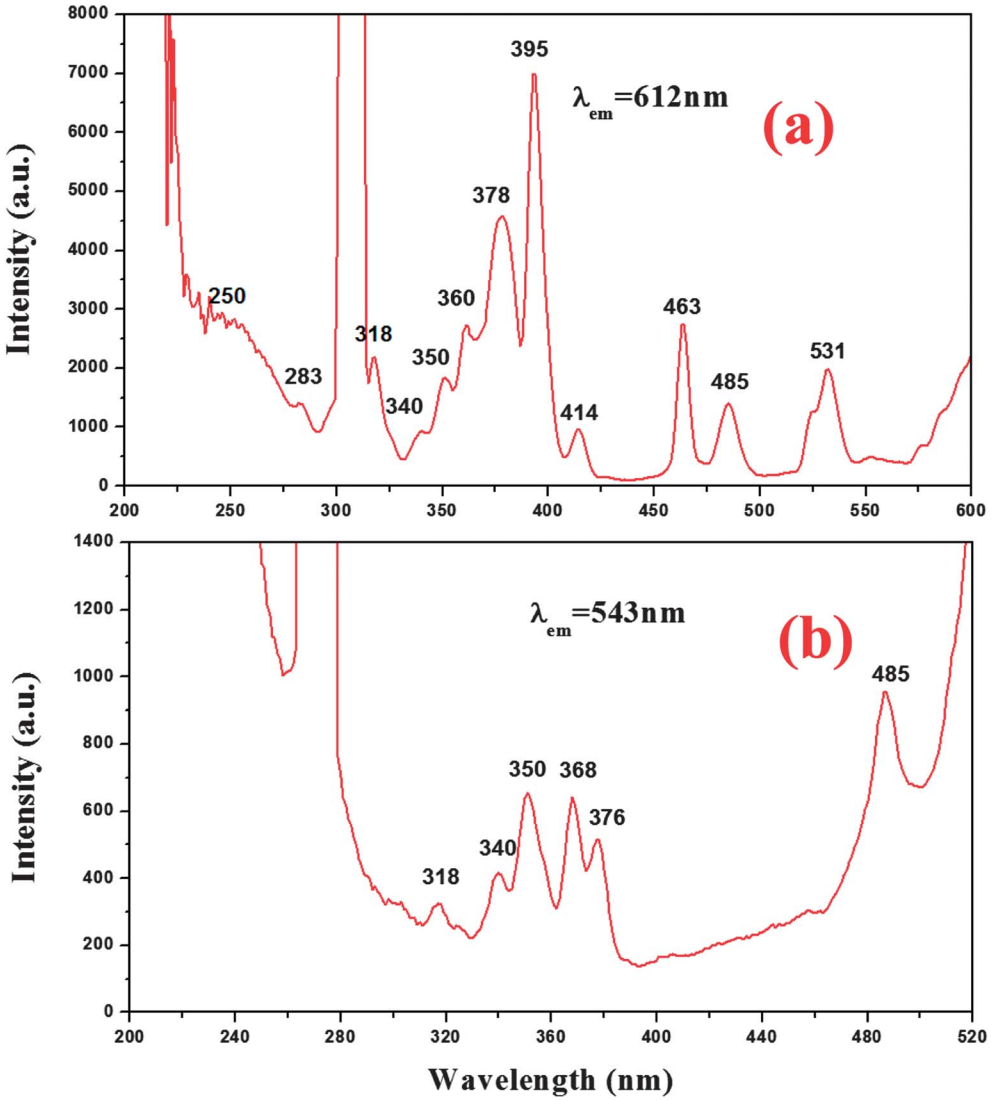

Fig. 7 The PLE spectra monitored at (a) 612 nm and (b) 543 nm, respectively.

electronic configurations of rare earth ions, and the electron transfer can happen between them when they are codoped in one host to reach a more stable configuration as the following process: Eu^{3+} ($4f^6$) + Tb^{3+} ($4f^8$) = Eu^{2+} ($4f^7$) + Tb^{4+} ($4f^7$).[51–53] It can be confirmed by the results of XPS, mentioned above. On the other hand, when Eu^{3+} ions are doped into the strontium germanate nanowires host lattice, the will replace the Sr^{2+} sites due to the smaller radius of Eu^{3+} (95 pm) and Tb^{3+} (92.5 pm) than that of Sr^{2+} (113 pm). However, as Eu^{3+} ions replace Sr^{2+} sites, charge balance is not satisfied. From the XPS results, it is clear that Eu^{2+} and Eu^{3+} ions coexist in the host lattice, indicating that some Eu^{3+} ions have been reduced to Eu^{2+} ions. As trivalent Eu^{3+} ions are doped into the $SrGe_4O_9$ host to replace Sr^{2+} ions, in order to maintain charge balance, one vacancy defect V''_{Sr} with two negative charges and two positive defects of $Eu_{Sr}^{\cdot}$ will be created by every two substitutions of Eu^{3+} ions in the strontium germanate nanowires host. The V''_{Sr} acts as the donor of electrons, while the two defects become acceptors of electrons. By thermal stimulation, the negative charges in vacancy defects will be transferred to Eu^{3+} sites and reduce Eu^{3+} to Eu^{2+}. These phenomena can be represented by followed equations:

$$2Eu^{3+} + 3Sr^{2+} \rightarrow 2Eu_{Sr}^{\cdot} + V''_{Sr} \quad (1)$$

$$V''_{Sr} = V^{x}_{Sr} + 2e' \quad (2)$$

$$2Eu_{Sr}^{\cdot} + 2e' = 2Eu^{x}_{Sr} \quad (3)$$

$$(1) + (2) + (3): 2Eu^{3+} + 3Sr^{2+} \rightarrow 2Eu^{x}_{Sr} + V^{x}_{Sr} \quad (4)$$

Fig. 8(f) is the emission spectrum of undoped strontium germanate nanowires under excitation at 280 nm. From it, a broad and intensive blue-violet emission centered at 400 nm was observed, which is considered to the Ge-related defect centers.[54–57] The blue emissions centered at 451 and 469 nm are believed to originate from the radiative recombination between an electron on oxygen vacancies and a hole on oxygen–germanium vacancy centers.[54–59] This demonstrates that the strontium

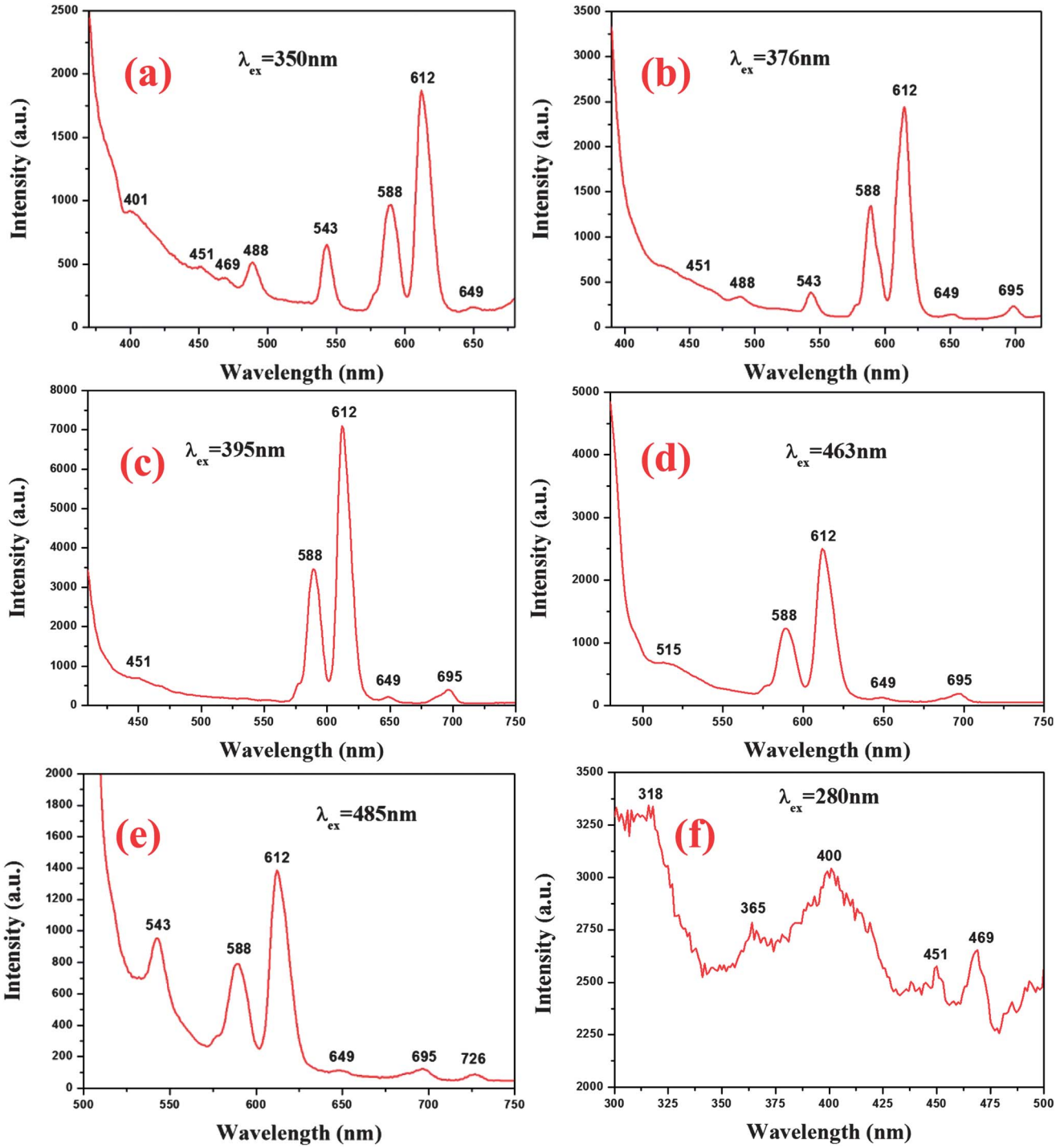

Fig. 8 The PL spectra of Eu^{3+}, Tb^{3+}-codoped strontium germanate nanowires under excitation at (a) 350 nm, (b) 376 nm, (c) 395 nm, (d) 463 nm and (e) 485 nm, respectively, and (f) the PL spectrum of undoped strontium germanate nanowires under excitation at 280 nm.

germanate nanowires make a significant contribution to the broad blue-violet emission band.

As discussed above, the obtained one-dimensional nano-phosphor can be excited effectively not only by UVLEDs but also by BLEDs. In order to prove this point, two emission spectra under excitation at 463 and 485 nm were given, as shown in Fig. 8(d) and (e), respectively. From the spectrum, the main emission peaks at 543, 588, 612, 649, 695 and 726 nm, can also be observed, which indicate that the obtained one-dimensional nano-phosphors can be excited by blue light.

It is well known that white emission can be realized by mixing the tricolor composition at a proper ratio.[60–63] Due to presenting simultaneously the Eu^{3+} and Tb^{3+} characteristic emission in the strontium germanate nanowire host, it is possible to realize the white emission in the strontium germanate nanowires host by codoping with Eu^{3+} and Tb^{3+} and

appropriately adjusting their concentrations. As can be seen in Fig. 8(a)–(e), with the change of excitation wavelength, the intensity ratio of the red, orange, green, blue-green and blue light changed. The corresponding CIE 1931 chromaticity coordinates are (0.376, 0.284), (0.455, 0.292), (0.485, 0.288), (0.399, 0.407) and (0.346, 0.468), under excitation at 350, 376, 395, 463 and 485 nm, respectively, as shown in Fig. 9, which are close to that of the standard white light point (0.33, 0.33). The excitation and emission spectra and the corresponding CIE 1931 chromaticity coordinates indicate that the Eu^{3+}, Tb^{3+}-codoped one-dimensional strontium germanate full color nano-phosphor can be excited effectively by near-ultraviolet light-emitting diodes (UVLEDs) and blue light-emitting diodes (BLEDs), and may have potential application as white-emitting phosphors in white-LEDs by carefully tuning the ratio of the Eu^{3+}/Tb^{3+}.

It is has been recognized that the luminescence intensities of various rare-earth ions can be enhanced or quenched by the energy transfer from other codoping rare-earth ions.[32,45,49–51] For example, an energy transfer can take place from Tb^{3+} to Eu^{3+} when they are codoped in one host, such as tungstates, hydrates, borates, zeolite-Y, yttria, porous silicon, and molybdates.[64–67] So far, little information is available on Eu^{3+}, Tb^{3+}-codoped one-dimensional strontium germanate full-color phosphors. So, we investigated the energy transfer properties in Eu^{3+}, Tb^{3+}-codoped one-dimensional strontium germanate full-color phosphors. As discussed above, it was found that not only the intra-4f transition characteristic absorption of Eu^{3+} but also the intra-4f transition characteristic absorption of Tb^{3+} can be observed in the excitation spectrum monitoring with the emission of Eu^{3+} at 612 nm, such as 301, 318, 340, 350, 368, 376 and 485 nm, which are correspond to $^7F_6 \rightarrow {}^3H_6$, $^7F_6 \rightarrow {}^5D_0$, $^7F_6 \rightarrow {}^5L_7$, $^7F_6 \rightarrow {}^5L_9$, $^7F_6 \rightarrow {}^5G_5$, $^7F_6 \rightarrow {}^5L_7$, $^7F_6 \rightarrow {}^5D_4$, respectively. This suggests that the excitation energy transfers effectively to Eu^{3+} in a radiationless transition manner after absorption by Tb^{3+}, which can enhance the $^5D_0 \rightarrow {}^7F_J$ transition of Eu^{3+}. If the energy transfer from Tb^{3+} to Eu^{3+} in the strontium germanate nanowires indeed occurs, the characteristic transitions of Eu^{3+} should appear in the emission spectrum of Eu^{3+}, Tb^{3+}-codoped strontium germanate nanowires when monitoring with 485 nm light. From the emission spectrum shown in Fig. 8(e), it can be observed that the emission spectrum simultaneously contains the 588 nm ($^5D_0 \rightarrow {}^7F_1$), 612 nm ($^5D_0 \rightarrow {}^7F_2$), 649 nm ($^5D_0 \rightarrow {}^7F_3$) and 695 nm ($^5D_0 \rightarrow {}^7F_4$) transitions of Eu^{3+} and the 543 nm ($^5D_4 \rightarrow {}^7F_5$) transition of Tb^{3+}, which further illustrates that Tb^{3+} ions may act as an energy donor in the strontium germanate nanowire host, in which excitation energy can be transferred to an acceptor Eu^{3+}. As mentioned above, when an energy transfer occurs between the codoping rare-earth ions in one host, the luminescence intensities of the rare-earth ions can be enhanced or quenched. To demonstrate, the emission spectra of the Eu^{3+}-doped and Eu^{3+}, Tb^{3+}-codoped strontium germanate nanowires under excitation at 395 nm were given, as shown in Fig. 10(a) and (b), respectively. The concentration of Eu^{3+} ions in the two samples is identical. Comparing 10(a) with 10(b), we found that the luminescence intensities of the 588 nm ($^5D_0 \rightarrow {}^7F_1$) and 612 nm ($^5D_0 \rightarrow {}^7F_2$) transitions of Eu^{3+} are enhanced over 134%. This further testifies the occurrence of energy transfer from Tb^{3+} to Eu^{3+}.

The decay time of Tb^{3+} ions also is a powerful tool to testify the energy transfer between Tb^{3+} and Eu^{3+} ions. Fig. 11 shows the respective decay curves for the luminescence of Eu^{3+} in Eu^{3+}, Tb^{3+}-codoped strontium germanate nanowires with different concentration of Eu^{3+} under excitation at 350 nm, monitored at 612 nm. It can be seen that the luminescence decay curves for $^5D_0$–$^7F_2$ (612 nm) of Eu^{3+} can be well fitted into a double-exponential function as the following equation:

$$I = A_1\exp(-t/\tau_1) + A_2\exp(-t/\tau_2) \quad (5)$$

where, I is the luminescence intensity; τ_1 and τ_2 are the fast and slow components of the luminescence lifetimes, A_1 and A_2 are the fitting parameters. The double-exponential decay behavior of the activator is often observed when the excitation energy is transferred from the donor to acceptor. The average lifetimes for $^5D_0$–$^7F_2$ (612 nm) of Eu^{3+} is calculated from the formula $\tau^* = (A_1\tau_1^2 + A_2\tau_2^2)/(A_1\tau_1 + A_2\tau^2)$, and the fitting results are shown in Table 1. Table 1 shows that the average lifetimes of Tb^{3+} ions in the Eu^{3+}, Tb^{3+}-codoped strontium germanate nanowires decreased with the increase of Eu^{3+} concentration. Based on the obtained experiment results, can be concluded that energy transfer from Tb^{3+} to Eu^{3+} ions occurs in the Eu^{3+}, Tb^{3+}-codoped strontium germanate nanowires.

As is known, there is a large number of various defects in the nanomaterials, which has a close relation with the material's optical properties. To investigate the correlation between the Eu^{3+}, Tb^{3+}-related green, orange and red emissions and the defect-related blue emission, we carried out comparative

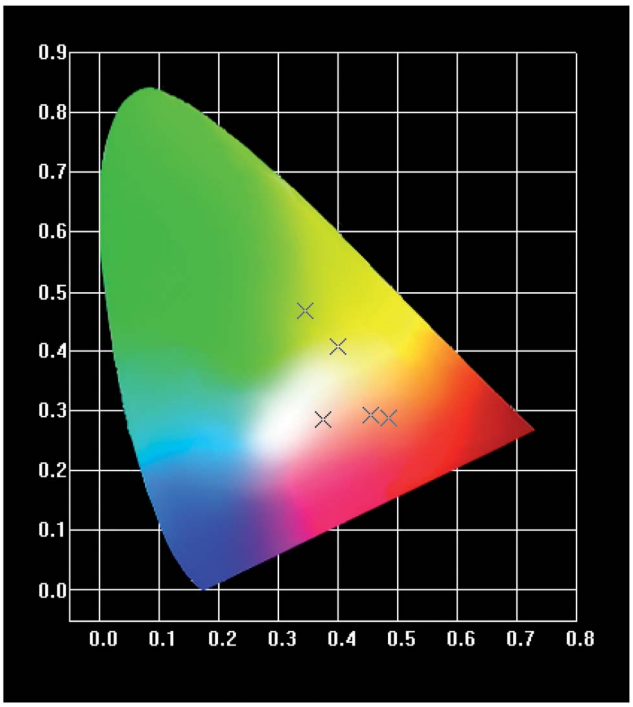

Fig. 9 The corresponding CIE 1931 chromaticity coordinates of The PL spectra under excitation at (a) 350 nm, (b) 376 nm, (c) 395 nm, (d) 463 nm and (e) 485 nm, respectively, as shown in Fig. 8.

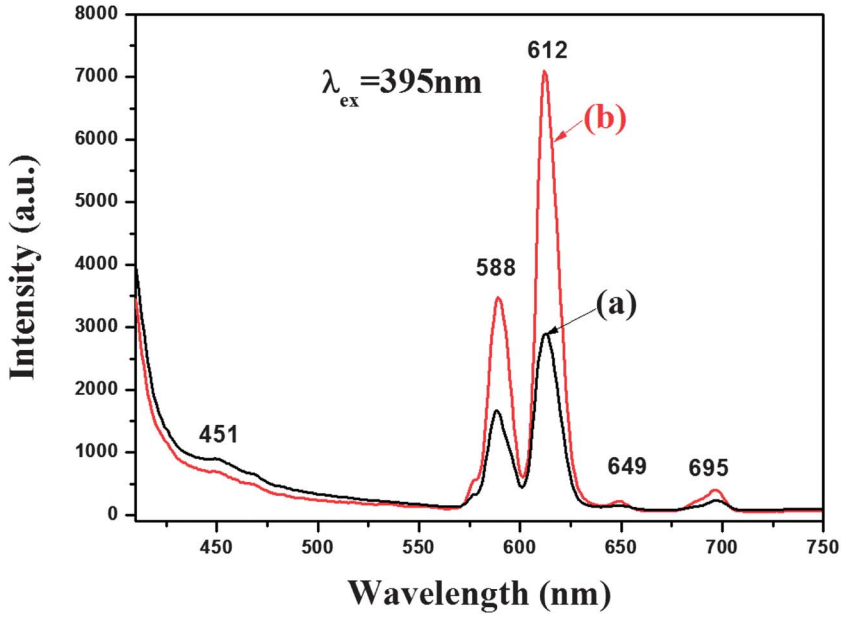

Fig. 10 The PL spectrum of (a) Eu^{3+}-doped and (b) Eu^{3+}, Tb^{3+}-codoped strontium germanate nanowires under excitation at 395 nm.

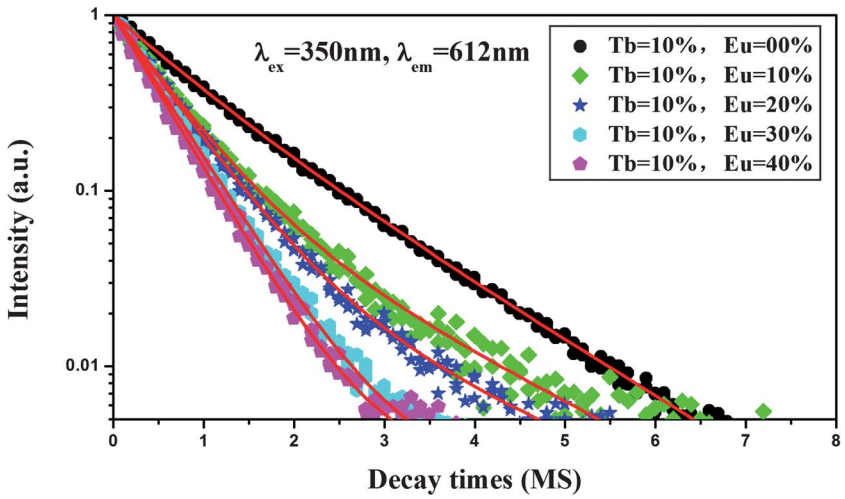

Fig. 11 Luminescence decay curves of Eu^{3+}, Tb^{3+}-codoped strontium germanate nanowires under 350 nm excitation, monitored at 612 nm.

measurements on a sample annealed at 400 °C in air for 1 h and the as-grown Eu^{3+}, Tb^{3+}-codoped strontium germanate nanowires and undoped strontium germanate nanowires, respectively. Fig. 12(a) shows the normalized emission spectra of the as-grown undoped strontium germanate nanowires (curve (1)) and Eu^{3+}, Tb^{3+}-codoped strontium germanate nanowires (curve (2)) samples under excitation at 280 nm. After doping, the characteristic emission band at 300–470 nm, originating from the oxygen vacancies and oxygen–germanium vacancies defect centers, became weaker, which suggests that these defect centers can be repaired by $Eu^{3+}$and Tb^{3+} ions, and weaken the characteristic emission of strontium germanate nanowires. It is noteworthy that the 395 and 463 nm photon are resonant with the $^7F_0 \rightarrow {}^5L_6$ and $^7F_0 \rightarrow {}^5D_2$ transitions of the Eu^{3+} ions, respectively, and the Eu^{3+}-related emission peak under the resonant excitation can be assigned to the $^5D_0 \rightarrow {}^7F_J$ ($J = 0, 1, 2, 3$) transitions, while the 340, 350, 368, 376 and 485 are resonant with the ($^7F_6 \rightarrow {}^5L_7$), ($^7F_6 \rightarrow {}^5L_9$), ($^7F_6 \rightarrow {}^5G_5$), ($^7F_6 \rightarrow {}^5G_6$) and ($^7F_6 \rightarrow {}^5D_4$) transition of the Tb^{3+} ions, respectively, and the Tb^{3+}-related emission peak under the resonant excitation can be assigned to the $^5D_4 \rightarrow {}^7F_5$ and $^5D_4 \rightarrow {}^7F_6$ transitions, as shown in Fig. 7. However, we also observed the orange (588 nm) and red (612 nm) emissions from the Eu^{3+} ions and blue-green (488 nm) and green (543 nm) emissions from the Tb^{3+} ions in the non-resonant excited spectra, although the emission is much weaker than the resonant case, as shown by curve (2) in Fig. 12(a). Such difference can be attributed to the fact that the resonant excitation directly excites the Tb^{3+} and Eu^{3+} ions, giving rise to a strong green and red emission. Under the NUV and blue excitation, only part of the Eu^{3+} and Tb^{3+} ions can

Table 1 The fitting results for the luminescence decay curves of the Eu^{3+}, Tb^{3+}-codoped strontium germanate nanowires with emission monitored at 612 nm

Eu^{3+} (mol%)	A_1	A_2	τ_1 (ms)	τ_2 (ms)	τ^* (ms)	R^2
00	242.53524	268.73966	1.40168	0.77620	1.16380	0.99906
10	0.843610	194.26755	8.21898	0.49504	1.01450	0.99677
20	1.063490	251.02558	7.63003	0.53251	0.93860	0.99670
30	18.92084	124.3648	1.63294	0.56648	0.89161	0.99805
40	8.259770	157.80831	1.99350	0.58198	0.79650	0.99740

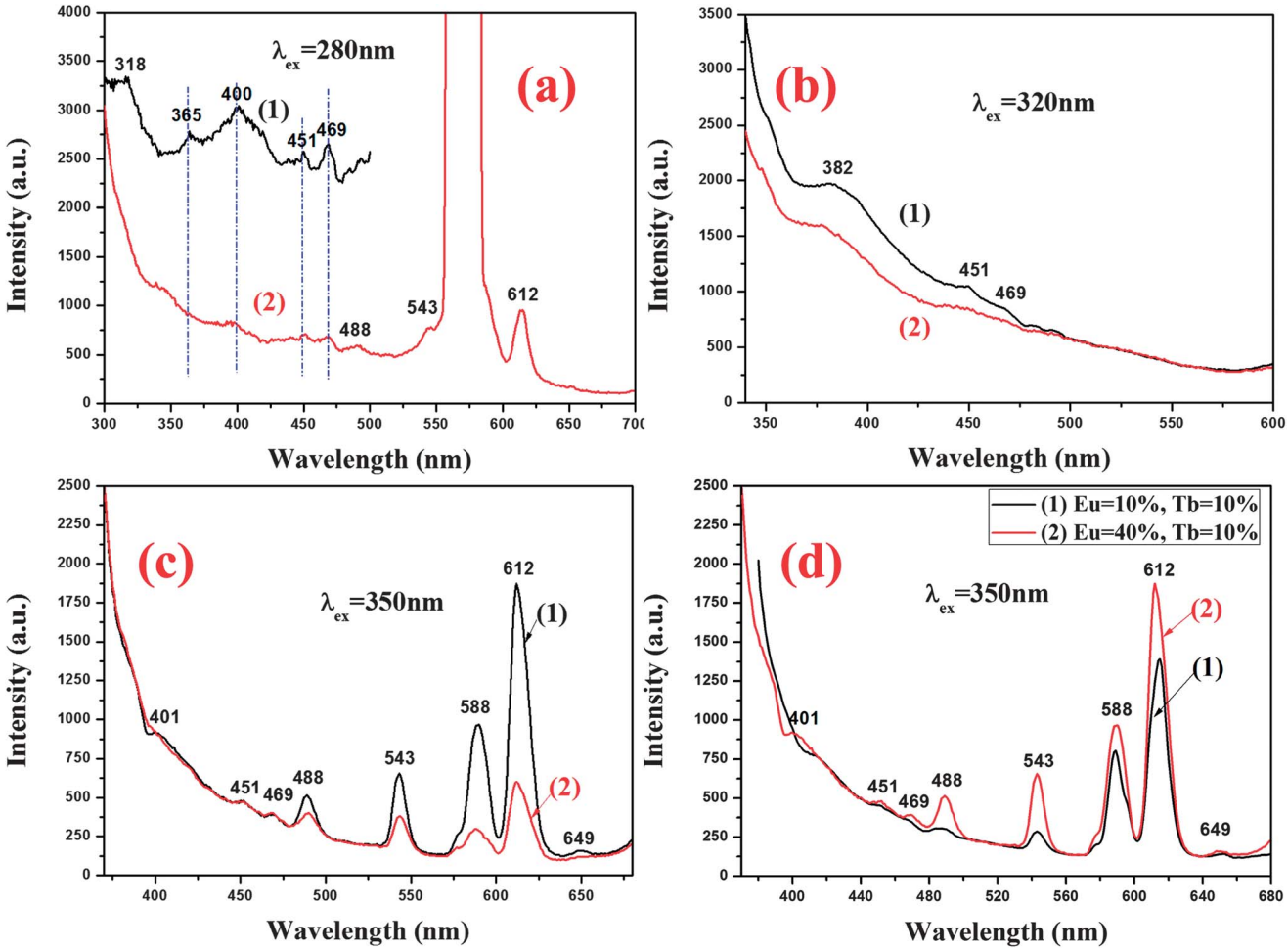

Fig. 12 The emission spectrum of (a) as-grown undoped (curve (1)) and Eu^{3+}, Tb^{3+}-codoped (curve (2)) strontium germanate nanowires under excitation at 280 nm; (b) as-grown (curve (1)) and annealed (curve (2)) undoped strontium germanate nanowires at 400 °C in air under excitation at 320 nm; (c) as-grown (curve (1)) and annealed (curve (2)) Eu^{3+}, Tb^{3+}-codoped strontium germanate nanowires at 400 °C in air under excitation at 350 nm; (d) as-grown Eu^{3+}, Tb^{3+}-codoped strontium germanate nanowires with different doping content under excitation at 350 nm (curve (1): Eu = 10%, Tb = 10%; curve (2): Eu = 40%, Tb = 10%).

absorb energy from the host and the energy transfer from the host is far less effective than the direct resonance absorption. Nevertheless, the observation of the Eu^{3+}, Tb^{3+}-related emission under the non-resonant conditions strongly suggests that there exists an energy transfer mechanism between the $SrGe_4O_9$ host and Eu^{3+}, Tb^{3+} ions, and below we will show that this energy transfer process is defect-mediated.

Fig. 12(b) shows the emission spectra of the as-grown (curve (1)) and annealed (curve (2)) strontium germanate nanowires under excitation at 320 nm. After annealing in air, the defect-related blue-violet characteristic emission band became weaker due to the decrease of the concentration of defects, such as oxygen vacancies and oxygen–germanium vacancies, which further suggest that the blue-violet emission is caused by the defects. Fig. 12(c) is the as-grown and annealed Eu^{3+}, Tb^{3+}-codoped strontium germanate nanowires with the 40% Eu^{3+} and 10% Tb^{3+}. After annealing, both the Eu^{3+}, Tb^{3+}-related green, orange and red emissions and the defect-related blue-violet emission at 401 nm are considerably quenched. This confirms that these defects (oxygen vacancies and

oxygen–germanium vacancies) can function as energy storage centers that mediate the energy transfer from the $SrGe_4O_9$ host to the Eu^{3+} and Tb^{3+} ions. However, the blue emission at 451 and 469 nm has no change. This indicated that the intrinsic defects (oxygen vacancies and oxygen–germanium vacancies) transfer to the defects caused by impurities (Eu^{3+} and Tb^{3+} ions) and further proved there are Eu^{2+} ions in the Eu^{3+}, Tb^{3+}-codoped strontium germanate nanowires which give rise to the blue emission, as mentioned above. Fig. 12(d) shows the emission spectra of as-grown Eu^{3+}, Tb^{3+}-codoped strontium germanate nanowires with different doping content. With the increase of doping content of Eu^{3+} ions, both the Eu^{3+}-related orange and red emission and Tb^{3+}-related green emissions are enhanced, while the defect-related blue-violet emission is almost unchanged, which further indicates that the storage energy by the defects in the host transfer to the Eu^{3+} and Tb^{3+} ions.

Based on the discussion above, we propose a possible energy transfer mechanism. Fig. 13 is the schematic illustrating the proposed mechanism of energy transfer among the host (a), Tb^{3+} (b) and Eu^{3+} (c). After excitation, the carriers are rapidly trapped at the defects or undergo subsequent band edge radiative emission. By means of a resonant energy transfer process, the trapped carriers at the defects could transfer their energy to the Eu^{3+} and Tb^{3+} ions, similar to the previous report on Eu-doped ZnO nanowires,[20] and finally enhance the characteristic emission of Eu^{3+} and Tb^{3+}. Compare (b) and (c), it can be observed that both the $^5D_0$ and $^5D_1$ energy levels of Eu^{3+} are located below the $^5D_4$ energy level of Tb^{3+}. In the case of Eu^{3+} ions, as the energy gap of $^5D_0 \rightarrow {}^7F_J$ ($J = 0$–6) is much larger than that of $^5D_{J+1} \rightarrow {}^5D^J$ ($J = 0$–3), therefore, the multiphonon relaxation process is predominant between the ^5D_J levels and radiative emission mainly occurs from the $^5D_0$ level to ^7F_J ($J =$ 0–6) in oxide hosts with higher phonon energy.[68] Therefore, when Eu^{3+} and Tb^{3+} codoped in a host and excited by near-ultraviolet or blue light, most of the excitation energy is transferred to the $^5D_3$ and $^5D_4$ levels of Tb^{3+} and the $^5D_0$, $^5D_1$, $^5D_2$ and $^5D_3$ levels of Eu^{3+}, which then give the characteristic emission of Tb^{3+} and Eu^{3+}. Meanwhile, some of the excitation energy of the $^5D_4$ energy level of Tb^{3+} transfers to the $^5D_1$ energy level of Eu^{3+}. Subsequently, the excitation energy transfers to the $^5D_0$ energy level of Eu^{3+} by energy relaxation and finally enhances the characteristic emission of Eu^{3+} at 590, 612, 649 nm and 695 nm. In other words, there is an energy transmission process between the Tb^{3+} and Eu^{3+}, as shown in Fig. 13(b) and (c).

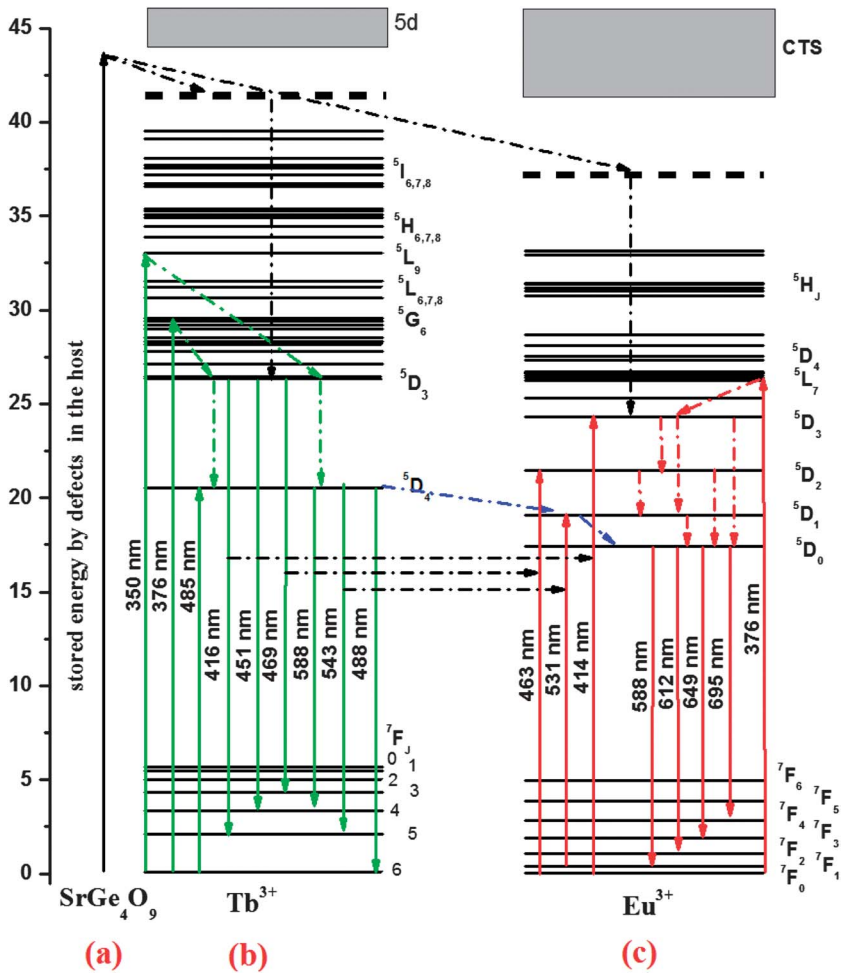

Fig. 13 Schematic illustrating the possible mechanism of energy transfer among the strontium germanate nanowires host, Eu^{3+} and Tb^{3+} ions and the energy level diagrams, visible emission transition for Eu^{3+} and Tb^{3+} ions.

Experiment section

Synthesis of Eu^{3+}, Tb^{3+}-codoped strontium germanate nanowires

The analytical reagents $C_4H_6O_4Sr \cdot 1/2H_2O$, Eu $(CH_3COO)_3$ and Tb $(NO_3)_3 \cdot 6H_2O$, and high-purity GeO_2 (99.99%) were purchased from Sinopharm Chemical Reagent Co., Ltd of China. All source materials were used without further purification. Stoichiometric amounts of the raw materials were weighed and dissolved in deionized water under vigorous stirring. After dissolving all the reactants, the solutions were then mixed in a 100 ml autoclave with a Teflon liner to form collosol. The collosol was sealed in the autoclave and maintained at 200 °C for 24 h. After the reaction and cooling to room temperature, the resulting white precipitates were filtered, washed with distilled water several times, until the pH of the water was equal to 7, and dried at 80 °C in air. After removing the excess reagents, a white powder was obtained. All the doped, codoped and undoped strontium germanate nanowires were obtained using the same method as mentioned above with different raw materials. The final products were used for the analysis of XRD, XPS, ICP-MS, SEM, TEM, HRTEM, Raman, FT-IR, PL, and so on.

Characterization

A JEOL JEM-2100F field emission high-resolution transmission electron microscope (HRTEM) with 1.9 point-to-point resolution operating with a 200 kV accelerating voltage, equipped with energy dispersive X-ray spectroscopy (EDX INCA, OXFORD), and a FEI Nova NanoSEM 230 field emission scanning electron microscope (FE-SEM) were used for the microstructure, morphological and chemical composition analysis. The FTIR spectra of the as-grown Eu^{3+}, Tb^{3+}-doped calcium germanate nanowires were obtained from a NEXUS 670 spectrometer in transmission mode at room temperature with a resolution of 4 and a scan frequency of 64. Photoluminescence (PL) and photoluminescence excitation (PLE) spectrum were measured with an F-4500 fluorescence spectrophotometer with a Xe lamp at room temperature. The excitation wavelength was 350–480 nm. The crystallinity and crystal structure of the as-prepared Eu^{3+}, Tb^{3+}-doped strontium germanate nanowires were carefully identified by XRD using a powder diffractometer (Rigaku D/Max-2550V) with graphite monochromatized Cu Ka radiation ($\lambda = 1.5406$ Å), and the XRD pattern was recorded in the range of $10^\circ \leq 2\theta \leq 80^\circ$ with a scanning step of 0.02° and counting time of 2 s per step. X-ray Photoelectron Spectroscopy (XPS) measurements were performed using an Al Kα micro-focused monochromator with a variable spot size of 30–400 μm in 5 μm steps (K-Alpha 1063, Thermo Fisher Scientific). The actual doping amount of Eu^{3+} and Tb^{3+} in the resulting materials was determined by inductively coupled plasma mass-spectrometry (ICP-MS) (Thermo Fisher X Series II).

Conclusion

In summary, a novel NUV and blue excitation Eu^{3+}, Tb^{3+}-codoped one-dimensional strontium germanate full-color nano-phosphor was synthesized successfully by a simple sol-hydrothermal method. The obtained one-dimensional nano-phosphors are single crystal nanowires with diameters between 10 and 80 nm, average diameter around 30 nm and length range from tens to hundreds of micrometers. The nano-phosphors showed intense blue, blue-green, green, orange and red or green, orange and red light emission under excitation at 350–380 nm and 485 nm, respectively. The energy transfer from the strontium germanate nanowire host (stored by defects in the host) to Tb^{3+} and Eu^{3+} ions and from the Tb^{3+} ions to Eu^{3+} ions are proposed. White-emission can be realized in a single-phase strontium germanate nanowire host by codoping with Tb^{3+} and Eu^{3+} ions. The Eu^{3+}, Tb^{3+}-codoped one-dimensional strontium germanate full-color nano-phosphors have superior stability under electron bombardment. The strong PL intensity, good CIE chromaticity and stability suggested that the obtained novel 1D full-color nano-phosphors have potential applications in W-LEDs.

Acknowledgements

This work was supported by the National Natural Science Foundation of China (Grant no. 51021063, 11165010), and the Planned Science and Technology Project of Hunan province (grant no. 2012FJ4331), and the China Postdoctoral Science Foundation funded project (Grant no. 2012M521539), and the Open-End Fund for the Valuable and Precision Instruments of Central South University (Grant no. CSUZC2012027), and the natural science foundation of Hunan Province (11JJ4045), the Training Program of Young Scientists (JingGang Star) in Jiangxi Province (No. 20133BCB23023).

References

1 F. Wang, D. Banerjee, Y. Liu, X. Chen and X. Liu, *Analyst*, 2010, **135**, 1839.
2 C. R. Ronda and T. Jüstel, *Luminescence: From Theory to Applications*, ed. C. R. Ronda, Wiley-VCH Verlag, Weinheim, Germany, 2008, ch. 2, pp. 35–59.
3 M. Higashi, R. Abe, K. Sayama, H. Sugihara and Y. Abe, *Chem. Lett.*, 2005, **34**, 1122.
4 T. Justel, H. Nikol and C. R. Ronda, *Angew. Chem., Int. Ed.*, 1998, **41**, 3084.
5 G. Hebbink, J. Stouwdam, D. Reinhoudt and E. Beggel, *Adv. Mater.*, 2002, **14**, 1147.
6 X. S. Yan, W. W. Li, X. B. Wang and K. Sun, *J. Electrochem. Soc.*, 2013, **159**(2), H195.
7 Y. S. Cho and Y. D. Huh, *Bull. Korean Chem. Soc.*, 2011, **32**(6), 2087.
8 J. H. Park, N. W. Jang, J. S. Kim and Y. S. Jeong, *Phys. Status Solidi B*, 2009, **246**(4), 897.
9 L. A. Diaz-Torres, P. Salas, J. S. Perez-Huerta, C. Angeles-Chavez and E. Dela Rosa, *J. Nanosci. Nanotechnol.*, 2008, **8**(12), 6425.
10 T. Erdem, S. Nizamoglu and H. V. Demir, *Conference on Light-Emitting Diodes: Materials, Devices, and Applications for Solid State Lighting XVI*, San Francisco, California, USA, 2012.

11 T. Matsumoto, J. Suzuki, M. Ohnuma, Y. Kanemitsu and Y. Masumoto, *Phys. Rev. B: Condens. Matter Mater. Phys.*, 2001, **63**(19), 195322.
12 K. Kawamura, T. Kidera, A. Nakajima and S. Yokoyama, *J. Phys. D: Appl. Phys.*, 2002, **91**(8), 5213.
13 C. Pichering, M. I. J. Beale, D. J. Robbins, P. J. Pearson and R. Greef, *Solid State Phys.*, 1984, **17**, 6535.
14 L. T. Canham, *Appl. Phys. Lett.*, 1990, **57**, 1046.
15 T. K. Sham, S. J. Naftel, P. S. G. Kim, R. Sammynaiken and Y. H. Tang, *Phys. Rev. B: Condens. Matter Mater. Phys.*, 2004, **70**, 045313.
16 D. P. Yu, Q. L. Hang, Y. Ding, H. Z. Zhang, Z. G. Bai, J. J. Wang, Y. H. Zou, W. Qian, G. C. Xiong and S. Q. Feng, *Appl. Phys. Lett.*, 1998, **73**, 3076.
17 L. W. Lin, *Nanoscale*, 2011, **3**, 1582.
18 L. W. Lin and Y. H. He, *CrystEngComm*, 2012, **14**, 3250–3256.
19 J. Lin, Y. Huang, J. Zhang, J. M. Gao, X. X. Ding, Z. X. Huang, C. C. Tang, L. Hu and D. F. Chen, *Chem. Mater.*, 2007, **19**, 2585.
20 D. D. Wang, G. Z. Xing, M. Gao, L. L. Yang and T. Wu, *J. Phys. Chem. C*, 2011, **115**, 22729.
21 D. L. Geng, G. G. Li, M. M. Shang, C. Peng, Y. Zhang, Z. Y. Cheng and J. Lin, *Dalton Trans.*, 2012, **41**(10), 3078.
22 E. T. Goldburt, B. Kulkarni, R. N. Bhargava, J. Taylor and M. Libera, *J. Lumin.*, 1997, **72–74**, 190.
23 G. Gwakefield, E. Holland, P. J. Dobson and J. L. Hutchison, *Adv. Mater.*, 2001, **13**, 1557.
24 H. W. Song, J. W. Wang, B. J. Chen, H. S. Peng and S. Z. Lu, *Chem. Phys. Lett.*, 2003, **376**, 1.
25 Z. G. Wei, L. D. Sun, C. S. Liao, J. L. Yin, X. C. Jiang and C. H. Yan, *J. Phys. Chem. B*, 2002, **106**, 10610.
26 X. Xu, T. Nishimura, Q. Huang, R. J. Xie, N. Hirosaki and H. Tanaka, *J. Am. Ceram. Soc.*, 2007, **90**(12), 4047.
27 M. M. Shang, G. G. Li, D. M. Yang, X. J. Kang, C. Peng, Z. Y. Cheng and J. Lin, *Dalton Trans.*, 2011, **40**, 9379.
28 C. K. Xu, M. Kim, J. Chun, D. E. Kim, B. Chon, S. Hong and T. Joo, *Scr. Mater.*, 2005, **53**, 949.
29 R. Q. Song, A. W. Xu and S. H. Yu, *J. Am. Chem. Soc.*, 2007, **129**, 4152.
30 L. Z. Pei, Y. Yang, C. G. Fan, C. Z. Yuan, T. K. Duan and Q.-F. Zhang, *CrystEngComm*, 2011, **13**, 4658.
31 Q. Liu, Y. Zhou, J. Kou, X. Chen, Z. Tian, J. Gao, S. Yan and Z. Zou, *J. Am. Chem. Soc.*, 2010, **132**, 14385.
32 M. J. Huang, X. Wang, Y. Hou, X. Chen, L. Wu and X. Fu, *Environ. Sci. Technol.*, 2008, **42**, 7387.
33 J. Huang, K. Ding, Y. Hou, X. Wang and X. Fu, *ChemSusChem*, 2008, **1**, 1011.
34 C. Yan, N. Singh and P. S. Lee, *Cryst. Growth Des.*, 2009, **9**, 3697.
35 L. Z. Pei, Y. Yang, Y. Q. Pei, C. Z. Yuan, T. K. Duan and Q. F. Zhang, *Cryst. Res. Technol.*, 2011, **46**, 480.
36 W. Li, Y. X. Yin, S. Xin, W. G. Song and Y. G. Guo, *Energy Environ. Sci.*, 2012, **5**, 8007.
37 C. J. Zhang, G. Tang and A. X. Lu, *J. Wuhan Univ. Technol., Mater. Sci. Ed.*, 2011, **33**(3), 1 (in Chinese).
38 M. K. Murthy and E. M. Kirby, *Phys. Chem. Glasses*, 1964, **5**, 144.
39 S. Sakka and K. Kamiya, *J. Non-Cryst. Solids*, 1982, **49**, 103.
40 H. Verweij and J. H. J. M. Buster, *J. Non-Cryst. Solids*, 1979, **34**, 81.
41 T. Furukawa and W. B. White, *J. Mater. Sci.*, 1980, **15**, 1648.
42 G. Laudisio, M. Catauro and G. Luciani, *Mater. Chem. Phys.*, 1999, **58**, 109.
43 M. Catauro and A. Marotta, *Thermochim. Acta*, 2001, **371**, 121.
44 M. Catauro and G. Laudisio, *J. Therm. Anal. Calorim.*, 1999, **58**, 617.
45 J. E. Shelby, *J. Am. Ceram. Soc.*, 1983, **66**, 414.
46 H. E. Hoefdraad, *J. Solid State Chem.*, 1975, **15**, 175.
47 G. S. Raju, H. C. Jung, J. Y. Park, B. K. Moon, R. Balakrishnaiah, J. H. Jeong and J. H. Kin, *Sens. Actuators, B*, 2010, **146**, 395.
48 J. K. Park, S. M. Park, C. H. Kim and H. D. Park, *J. Mater. Sci. Lett.*, 2011, **20**, 2231.
49 C. F. Zhu, X. L. Liang, Y. X. Yang and G. R. Chen, *J. Lumin.*, 2010, **130**, 74.
50 X. M. Zhang, W. L. Li, L. Shi, X. B. Qiao and H. J. Seo, *Appl. Phys. B*, 2010, **99**, 279.
51 Y. Wu and C. S. Shi, *J. Alloys Compd.*, 1995, **224**, 177.
52 Y. Gao and C. S. Shi, *J. Phys. Chem. Solids*, 1996, **57**(9), 1303.
53 Y. Wu and C. S. Shi, *Solid State Commun.*, 1995, **95**(5), 319.
54 Z. Jiang, T. Xie, G. Z. Wang, X. Y. Yuan, C. H. Ye, W. P. Cai, G. W. Meng, G. H. Li and L. D. Zhang, *Mater. Lett.*, 2005, **59**(4), 416.
55 M. Zacharias and P. M. Fauchet, *J. Non-Cryst. Solids*, 1998, **230**(2), 1058.
56 M. Y. Tsai and T. P. Perng, *The 214th Electrochemical Society Meeting*, Honolulu, HI, USA, 2008, p. 12.
57 M. Y. Tsai, C. Y. Yu and T. P. Perng, *J. Nanosci. Nanotechnol.*, 2008, **8**, 6376.
58 Y. Y. Tay, T. T. Tan, F. Boey, M. H. Liang, J. Ye, Y. Zhao, T. Norby and S. Li, *Phys. Chem. Chem. Phys.*, 2010, **12**, 2373.
59 K. Dileep, L. S. Panchakarla, K. Balasubramanian, U. V. Waghmare and R. J. Datta, *Appl. Phys.*, 2011, **109**, 063523.
60 R. C. Evans, L. D. Carlos, P. Douglas and J. Rocha, *J. Mater. Chem.*, 2008, **18**, 1100.
61 H. C. Li, Y. P. Lin, P. T. Chou, Y. M. Cheng and R. S. Liu, *Adv. Funct. Mater.*, 2007, **17**, 520.
62 J. D. Ghys, R. Mauricot, B. Caillier, P. Guillot, T. Beaudette, G. H. Jia, P. A. Tanner and B. M. Cheng, *J. Phys. Chem. C*, 2010, **114**, 6681.
63 J. W. Wang and P. A. Tanner, *J. Lumin.*, 2008, **128**, 1846.
64 W. W. Holloway, M. Kestigian and R. Newman, *Phys. Rev. Lett.*, 1963, **11**, 458.
65 W. Chen, R. Sammynaiken and Y. Huang, *J. Appl. Phys.*, 2000, **88**, 1424.
66 J. Yang, C. M. Zhang, C. X. Li, Y. N. Yu and J. Lin, *Inorg. Chem.*, 2008, **47**, 7262.
67 M. M. Shang, G. G. Li, X. J. Kang, D. M. Yang, D. L. Geng and J. Lin, *ACS Appl. Mater. Interfaces*, 2011, **3**, 2738.
68 V. V. Ravi Kanth Kumar, A. K. Bhatnagar and R. Jagannathan, *J. Phys. D: Appl. Phys.*, 2001, **34**, 1563.